[3] Robben, F., Kunkel, W. B., and Talbot, L., "Spectroscopic Study of Electron Recombination with Monatomic Ions in a Helium Plasma," *Physical Review*, Vol. 132, No. 6, 1963, pp. 2363-2371.

[4] Talbot, L., Chou, Y. S., and Robben, F., "Expansion of a Partially-Ionized Gas Through a Supersonic Nozzle," Rept. AS-65-14, Aug. 1965, Univ. of California, Berkeley, Calif.

[5] Chou, Y. S. and Talbot, L., "Source-Flow Expansion of a Partially Ionized Gas into a Vacuum," *AIAA Journal*, Vol. 5, No. 12, Dec. 1967, pp. 2166-2172.

[6] Love, E. S., Grigsby, C. E., Lee, L. P., and Woodling, M. J., *Experimental and Theoretical Studies of Axisymmetric Free Jets*, TR R-6, 1959, NASA.

[7] Owen, P. L. and Thornhill, C. K., *The Flow in an Axially Symmetric Supersonic Jet from a Nearly Sonic Orifice into a Vacuum*, Rept. 30/48, 1948, Ministry of Supply, Armament Research Establishment, Great Britain.

[8] Jenkins, R. C., *Electrostatic Probe Measurements in a Partially Ionized Free Jet from a Sonic Orifice*, Rept. RE-333, July 1968, Grumman Research Dept., Grumman Aerospace Corp., Bethpage, N.Y.

[9] Sonin, A. A., "Free-Molecule Langmuir Probe and Its Use in Flowfield Studies," *AIAA Journal*, Vol. 4, No. 9, Sept. 1966, pp. 1588-1596.

[10] Graf, K. A., *The Determination of Spatially Non-Uniform Electron Density Distribution*, UTIAS Rept. 108, April 1965, Univ. of Toronto.

[11] Ashkenas, H. and Sherman, F. S., "The Structure and Utilization of Supersonic Free Jets in Low Density Wind Tunnels," *Rarefied Gas Dynamics*, Vol. II, edited by J. Laurmann, Academic Press, New York, 1963, Sec. 7,

[12] Bray, K. N. C., "Electron-Ion Recombination in Argon Flowing Through a Supersonic Nozzle," AGARDograph 68, 1963, pp. 67-87.

[13] Wilson, J. A., Ph. D. thesis, 1962, Univ. of Southhampton, England.

[14] Bates, D. R. and Kingston, A. E., "Properties of a Decaying Plasma," *Planetary and Space Science*, Vol. 1, No. 11, 1963, pp. 1-22.

[15] Kerrebrock, J. L., "Magnetohydrodynamic Generators with Nonequilibrium Ionization," *AIAA Journal*, Vol. 3, No. 4, April 1965, pp. 591-601.

[16] Norman, W., *One-Dimensional Magnetohydrodynamic Equations for a Non-Ideal Gas with Application to Singly Ionizing Argon*, AEDC-TR-65-185, Arnold Engineering Development Center, Arnold Air Force Station, Tenn, 1965.

[17] Christiansen, W. H., "Study of Shock Waves in a Nonequilibrium Plasma," *The Physics of Fluids*, Dec. 1967, pp. 2586-2595.

JULY 1971 AIAA JOURNAL VOL. 9, NO. 7

# A Variable Phase Velocity Traveling Wave Pump

CHARLES W. HALDEMAN,* JOHN P. SULLIVAN,† AND EUGENE E. COVERT‡
*Massachusetts Institute of Technology, Cambridge, Mass.*

**Results of analytical and experimental studies of an electrodeless, alternating-current plasma accelerator, the traveling wave pump, are presented. A coil assembly that produces a variable phase velocity and eliminates end effects is used. Data is presented indicating supersonic acceleration of argon plasma in qualitative agreement with the mathematical model.**

## Nomenclature

$r,\theta,z$ = circular cylindrical coordinates
$A_\theta$ = azimuthal component of vector potential
$\hat{a}_r,\hat{a}_\theta,\hat{a}_z$ = unit vectors
$a$ = speed of sound
$\mathbf{B}$ = magnetic flux density
$B_{\text{eff}}$ = effective amplitude of magnetic flux density; $0.5\text{-}(\mu NI)^2(kr_0)^2K_1^2(kr_0)[I_1^2(kr_0) - I_0(kr_0)I_2(kr_0)] = B_{\text{eff}}^2$
$C$ = capacitance per unit length
$\mathbf{E}$ = electric field
$G$ = Green's function
$I$ = current per turn in exciting coil
$I_n(x)$ = modified Bessel function of the first kind of order $n$ and argument $(x)$
$\mathbf{J}$ = current density
$J_n(x)$ = Bessel function of the first kind of order $n$ and argument $(x)$
$\mathbf{K}$ = current sheet intensity
$K_n(x)$ = modified Bessel function of the second kind of order $n$ and argument $(x)$
$k$ = wave number
$k_n$ = $\lambda n/R$
$L$ = inductance per unit length, length
$M$ = Mach Number
$M_0$ = initial Mach Number
$N$ = number of turns per unit length on exciting coil
$P$ = pressure
$P_0$ = isentropic stagnation pressure
$R$ = radius of channel, resistance
$T$ = temperature
$t$ = time
$u$ = velocity
$\bar{u}$ = time averaged component of velocity
$u_0$ = initial velocity
$u'$ = unsteady component of velocity
$V_p$ = phase velocity of magnetic wave $V_p = \omega/k(z)$
$z$ = axial position $(m)$
$\gamma$ = ratio of specific heats
$\lambda_n$ = $n$th root of $J_0(x) = 0$
$\mu$ = magnetic permeability = $4\pi \times 10^{-7}$ $h/m$ in free space
$\xi$ = length parameter $\xi = \int(\sigma B_{eff}^2/\rho u)dz$
$\rho$ = mass density
$\sigma$ = electrical conductivity
$\omega$ = angular frequency

Received September 23, 1970; revision received March 23, 1971. This investigation was sponsored by the Aerospace Research Laboratories, Air Force Systems Command, U.S. Air Force, under Contract F33615-68-C-1380, and the Microwave Physics Laboratory, Air Force Cambridge Research Laboratories, Office of Aerospace Research, U.S. Air Force, under Contract F19628-69-C-0043.

* Associate Director, Aerophysics Laboratory. Member AIAA.

† Research Assistant, Department of Aeronautics and Astronautics.

‡ Professor. Associate Fellow AIAA.

## Introduction

IN the classic rocket or wind-tunnel propulsion system, the enthalpy of the working fluid is converted to velocity (or Mach number) by an adiabatic expansion through a deLaval

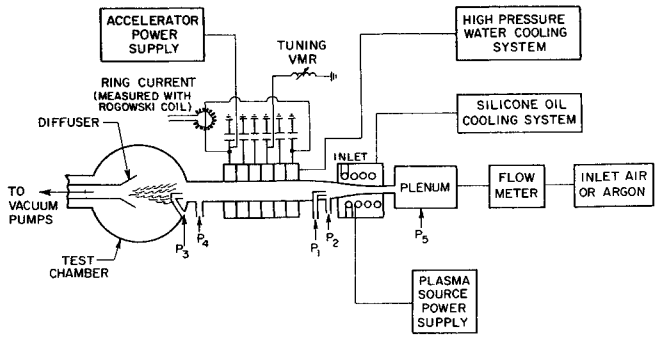


**Fig. 1 Diagram of plasma source and accelerator setup.**

nozzle. Clearly, as a higher velocity or Mach Number is desired, the initial pressure and enthalpy become higher, giving rise to a number of problems which have limited the attainable Mach number. One alternate process is the use of the Lorentz body force ($\mathbf{J} \times \mathbf{B}$) for this purpose. This force may be developed using direct currents and steady fields, or by using alternating currents. The latter alternative has been selected for these studies. It was shown initially[1] that a traveling wave current sheet in a conductor surrounding a gas could drive the gas. Subsequently it was shown[2] that, on the average, the traveling wave machine was comparable to the direct current machine whose characteristic speed is $\mathbf{E}/\mathbf{B}$. Indeed the critical points in the flow discussed by Sears and Ressler[3] and the effects of viscosity discussed by Dahlberg[4] can be identified at once in the traveling wave machine. The results from Sears and Ressler and from Dahlberg indicate the possibility of increasing the velocity by this means. For wind-tunnel use, it is desirable to increase the Mach Number simultaneously, a more difficult goal because $I^2R$ losses in the accelerating gas tend to increase its temperature and hence reduce Mach number. Previous theoretical results[1-4] show circumstances where the Mach number and velocity are simultaneously increased.

The purpose here is to describe an experimental arrangement, (shown in Fig. 1) including a 42mHz plasma source[5] and a variable phase velocity§ end shielded accelerator coil,[6] and to present experimental results indicating significant increase in observed Mach number not incompatible with theoretical predictions. These results at supersonic Mach numbers extend earlier results[7] at subsonic Mach Numbers.

## Mathematical Model

The simplicity of a one-dimensional model in the preliminary analysis[1-4] suggests its continued use. The one-dimensional equations of motion are: (the magnetic forcing terms for an accelerator with variable phase velocity are derived in the Appendix)

$$\partial\rho/\partial t + u\partial\rho/\partial z + \rho\partial u/\partial z = 0$$

$$\rho\frac{\partial u}{\partial z} + \rho u\frac{\partial u}{\partial z} + \frac{\partial p}{\partial z} = \sigma B_{\text{eff}}^2(V_p - u)\left\{1 - \cos 2\left[\int_0^z k(\xi)d\xi - \omega t\right]\right\}$$

$$\frac{\partial p}{\partial t} + \gamma p\frac{\partial u}{\partial z} + u\frac{\partial p}{\partial z} = (\gamma - 1)\sigma B_{\text{eff}}^2(V_p - u)\left\{1 - \cos 2\left[\int_0^z k(\xi)d\xi - \omega t\right]\right\}$$

Assuming there is a solution consisting of a steady mean flow plus a small time varying flow, i.e., let $\bar{u}(x,t) = \bar{u}(x) + u'(x,t)$ etc., the zero-order time averaged equations become

$$\frac{1}{u}\frac{du}{dz} = \frac{\sigma B_{\text{eff}}^2}{\rho u}\frac{\gamma M^2}{M^2 - 1}\frac{1}{(u/v_p)^2} \times \left(1 - \frac{u}{V_p}\right)\left(\frac{u}{V_p} - \frac{\gamma - 1}{\gamma}\right) \quad (1)$$

$$\frac{1}{M}\frac{dM}{dz} = \frac{\sigma B_{\text{eff}}^2}{\rho u}\frac{\gamma M^2}{M^2 - 1}\left(1 + \frac{\gamma - 1}{2}M^2\right)\frac{1}{(u/V_p)^2} \times \left\{\left(1 - \frac{u}{V_p}\right)\left(\frac{u}{V_p} - \frac{(\gamma - 1)/2\gamma + [(\gamma - 1)/2]M^2}{1 + [(\gamma - 1)/2]M^2}\right)\right\} \quad (2)$$

Equations (1) and (2) are the same as those derived by Resler and Sears[3] with $V_p = E/B$ and $B_{\text{eff}} = B$, and in general must be integrated numerically. However, if $u/V_p$ is a function of Mach number only, then Eqs. (1) and (2) can be integrated exactly. In three cases of interest, $u/V_p$ is such a function and exact relations can be found.[8] These are maximum $P_0$ (isentropic stagnation pressure) increase, maximum Mach number increase and constant temperature. These solutions illustrate the very important fact that the thermodynamic process in the accelerator can be controlled by prescribing the axial distribution of phase velocity.

The function $u/V_p$ that leads to the maximum increase in $P_0$ is found by setting $d/d(u/V_p)(dP_0/dz) = 0$. Straightforward manipulation gives the solution

$$u/V_p = 1/\{1 + [1/(\gamma - 1)M^2]\}$$

$$u/u_0 = (M/M_0)^2 = [\xi/(\gamma - 1)M_0^2] + 1$$

$$V_p/u_0 = \xi/(\gamma - 1)M_0^2 + [1 + (\gamma - 1)M_0^2]/(\gamma - 1)M_0^2$$

where $\xi$ is the integrated interaction length.

The other cases have been treated in a similar manner. The results are shown in Figs. 2 and 3. The maximum $P_0$ case was chosen as the basis for initial experiments since the energy added per unit length is greatest, thus reducing the length of the device, while the Mach numbers obtainable are within 4% (at least up to $M = 10$) of the maximum Mach Number case. Further, if the interaction parameter $\sigma B_{\text{eff}}^2/\rho u$ is constant, the phase velocity $V_p$ is a linear function of distance along the accelerator $z$. This simplifies the construction of the coil assembly for the accelerator.

The solution of the first-order equations under the WKBJ approximation that $(V_p)^{-1}\, dV_p/dz$ is small (slowly varying wave speed) suggests the approximate solution fails near

$$u = V_p \pm a$$

where $a$ is the local speed of sound.[9-11] In any event, use of an accelerating wave allows one to control the difference in velocities and so avoid this condition.

## Coil System

Having selected the maximum $P_0$ process which implies a linearly increasing phase velocity (Fig. 2), the next step is the design of a coil assembly to give the required fields. The coils will be used as a slow transmission line[6] rather than as a polyphase system. A polyphase system has been used by See-

§ In an acceleration device where the phase velocity $V_p$ is constant along the channel, the gas can be accelerated only to a velocity approaching $V_p$, since at this point the $\mathbf{J} \times \mathbf{B}$ force will equal zero. At first this does not seem to be a large restriction, but examination of the power addition reveals that the acceleration that can be achieved is limited. For example, under the assumption of scalar conductivity, the power added to the gas is given by $\mathbf{E}\cdot\mathbf{J} = \mathbf{J}^2/\sigma + \mathbf{u}\cdot\mathbf{J} \times \mathbf{B}$, where $\mathbf{J}^2/\sigma$ represents heat addition and $\mathbf{u}\cdot\mathbf{J} \times \mathbf{B}$ represents direct energy addition. To add mostly kinetic energy, $(\mathbf{u}\cdot\mathbf{J} \times \mathbf{B})/\mathbf{E}\cdot\mathbf{J}$, should be close to 1. However, for an idealized process where $\mathbf{u}$ is axial and uniform. the ratio of $(\mathbf{u}\cdot\mathbf{J} \times \mathbf{B})/\mathbf{E}\cdot\mathbf{J} = u/V_p$. Thus if $u/V_p$ at the inlet is equal to 0.8, the velocity can only be increased by 20%. However, if $V_p$ is increased along the channel, the change in gas velocity seems limited only by the power available.

mann, et al.[7] A Fourier analysis of their three-phase coil system[13] shows the strong effects of harmonics, which are difficult to eliminate.¶

A transmission line terminated in its characteristic impedance, or operating in the ring mode (see below) produces a wave traveling with a phase velocity $V_p = (LC)^{-1/2}$, where $L$ is the inductance per unit length and $C$ is the capacitance per unit length. By varying $L$ and $C$ with length, the phase velocity can be varied. The inductance is varied by changing the number of turns of the individual coils; the capacitance being varied by simply changing the value of the external capacitors.

Slow transmission line coil systems have been under study since the early work on the accelerator[1]; however, until the present paper, the theoretical work dealt with infinitely long, constant phase velocity models with and without magnetic core structures.[6,9,12] Calculation of the inductance of such a long, slow wave structure was performed by energy methods using the magnetic fields for the infinite length case. Use of this value for the inductance accurately reproduced the experimentally observed dependence of $V_p$ (phase velocity) on $kR_0$, however, the measured phase velocity of the structure was always higher than the calculated value even when measured far from the ends on long ($L/D = 20$) models. This effect was observed for both distributed energy storage coils with built in distributed capacitance and lumped parameter circuits with external capacitance which ranged in phase velocity from 60,000 to 2000 m per sec.

For a multiple coil array like the present accelerator coil system, the most accurate approach would be to include all self and mutual inductances for the 22 coil array leading to a $22 \times 22$ matrix. Solution of this theoretical system should yield accurate phase velocity as well as terminal properties and reduce the need for cut and try tuning to achieve the desired operating mode.

Since time did not permit solution of this analytical model, the coil turns distribution was determined from the required coil inductance for a long slow wave coil.[12]

It has been found[6,14] that in order to produce a wave of variable velocity, the ratio $L/C$ must be maintained constant along the coil, i.e., constant characteristic impedance.

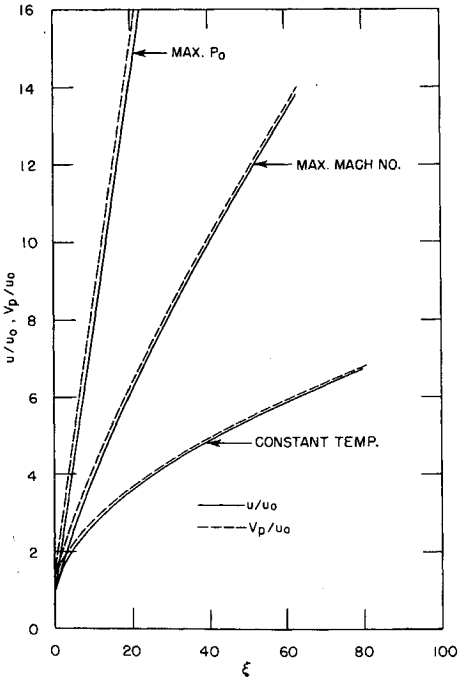


**Fig. 2** $u/u_0$ **and** $V_p/u_0$ $\xi = \int (\sigma B^2_{\text{eff}}/\rho u)dz$.

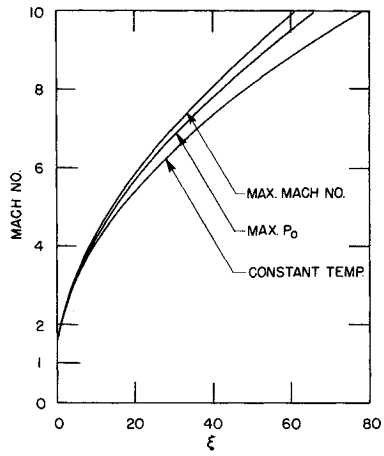


**Fig. 3 Mach number vs** $\xi = \int (\sigma B^2_{\text{eff}}/\rho u)\, dz$ **with** $M_0 = 1.5$

Because high magnetic energy densities are required to achieve the magnetic field levels useful for plasma acceleration, a considerable effort has been devoted to the construction of high-power, low-loss coils for the accelerator. The design selected for the acceleration coils is shown in Fig. 4. A series of "pancake"-type coils, rather than a thicker coil, was chosen to obtain the smallest practical coil length compared to the wavelength of the traveling magnetic wave. Earlier experiments[6,14] had indicated that for a series of coils and capacitors to behave like a slow transmission line electrically, and at the same time produce a smooth magnetic field inside the coil array, individual coil length must be small compared to both the wavelength of the traveling field and the coil inside diameter.

Special techniques for constructing high-power coils have been developed using very fine Litz cable with internal cooling. Peak quality factors ($\omega L/R$) for single pancakes ranged from 600 to 1200. These coils using nylon cooling tubes have been operated at 400 amp rms (240,000 amp turns per meter) at 30kc using 200 psi tap water for cooling. A sample coil with the internal cooling channel enlarged by chemically removing the tube wall was operated at 1040 amp (625,000 amp turns per meter equivalent).

Figure 5 shows the final design of the coil assembly. It consists of twenty-two** coils ranging from 10 to 5 turns. The turns are distributed to give a phase velocity that approximates a linear increase along the channel. In the traveling wave region, the phase velocity is given by

$$V_p/V_{pi} = 3(z/0.266) + 1$$

where $z$ is in meters and $V_{pi}$ is the phase velocity at the inlet and is varied by changing the over-all capacitance level of the system. It should be noted that with additional coils, a phase velocity variation corresponding to either the maximum Mach number or constant temperature case could be produced without difficulty.

An electrical schematic for the coil system operating in the ring mode is shown in Fig. 1. The connection point to insure a traveling mode on the accelerator was found by a trial and error process. Choosing the proper point of excitation on the coil, adjusting a variometer at the inlet end, and "trimming" the capacitors on the accelerator resulted in the desired traveling mode. The relative field amplitude and phase (relative to fixed reference) of a pickup coil traversed along the coil axis is shown in Fig. 6. The phase velocity calculated from this phase measurement is shown in Fig. 7. The difference between the actual phase velocity and the linearly increasing

¶ Because of an error in this and earlier dated references, the reported conductivities should be *halved*, i.e., where $(\mu NI)^2/4$ occurs it should be $(\mu NI)^2/2$. References 6, 10 and 14 are correct.

** Because of a shortage of high-power capacitors, the high-power experiments were carried out with only 20 coils.

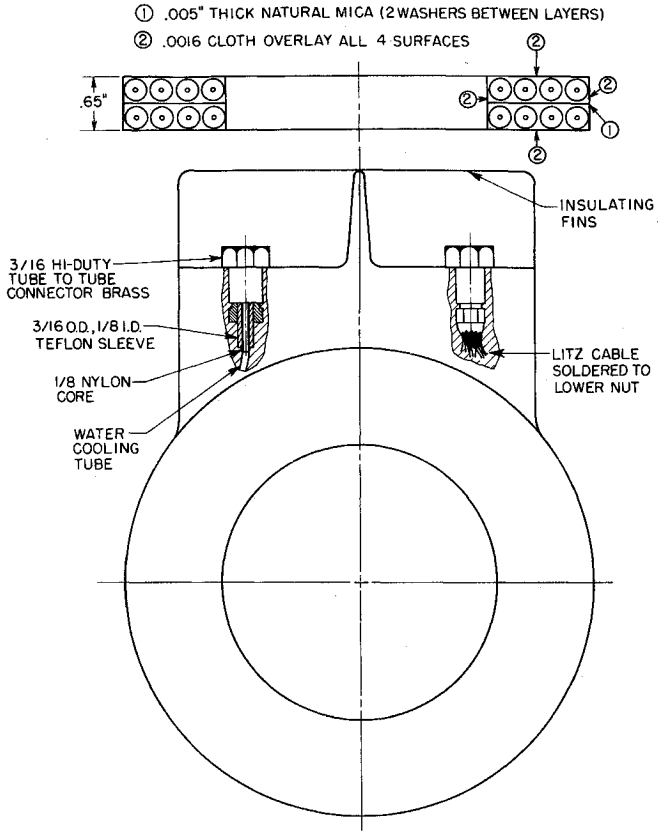


**Fig. 4 Sample high-power coil winding geometry using 0.300 diam 12,000/46 Litz cable.**

design phase velocity is a result of the long coil inductance used to design the coils. By reducing the inductance (i.e., number of turns) of the coils near the center of the system, this effect can be overcome. The experimental measurements, Fig. 7, indicate that $V_p$ is extremely large in the inlet region. In fact, there is a standing wave ($V_p = \infty$) about one-half of a diameter upstream of the first coil. This causes $u/V_p \to 0$, which implies excessive joule heating. To prevent this, a copper shield is placed between the end coils and the plasma to shield the plasma from the fringing field. The effectiveness of this shield is shown in Fig. 6. The copper shield seems to be a simpler way of eliminating end effect than construction of the two-coil shading system described by Fanucci and Jester.[15]

## Description of the Experiment

The basic equipment (shown in Fig. 1) consists of the RF plasma source (operated at a frequency of 42mHz), a nozzle, the traveling wave pump (operating at a frequency of 34KHz), a test chamber, diffuser and vacuum system. The plasma flow channel is formed by a silicone oil cooled quartz DeLaval nozzle in the plasma source region connecting to the 3.2-in. constant diameter†† water-cooled quartz accelerator section.

The available instrumentation includes Stokes-McLeod vacuum gauges ($P_2$,$P_3$,$P_4$), a Wallace and Tiernan dial manometer, 0–20 Torr ($P_1$), and a CVC pressure gauge, 0–300 Torr ($P_5$). (The location of pressure taps is shown in Fig. 1.) In addition to pressures, the mass flow and temperature rise of cooling water for the plasma tube and silicone fluid for the plasma source nozzle were measured using variable area flow meters and ten junction thermopiles.

Electrical variables were measured with the power supply panel meters and Tektronix 502 oscilliscopes. The frequency of operation was continuously displayed on a digital frequency counter. Mass flow of argon through the system was metered with a Fischer-Porter "Flowrator" and high-sensitivity pressure gauge.

During experimental operation, the flow of argon was first established at the desired rate. The RF plasma source was then brought up to the desired power level and adjusted for stable operation and best plasma condition. After about 5 min to stabilize the temperature readings, a set of data was recorded. This process required about another 5 min. The accelerator was then brought up to the desired power level and after another period of about 5 min readings were again taken. The reduced data obtained from these initial runs of the accelerator are given in Table 1. Since information about the composition of the plasma was not available, the pressure data has been reduced assuming $\gamma = 1.2$ and 1.67. These two results are tabulated in Table I thus bracketing the true value of $\gamma$ which must lie somewhere in between.

The one-dimensional model[2] was extended to include variable phase velocity, viscosity, heat transfer and equilibrium real gas properties. A computer program was written to solve these equations numerically.

The local magnetic forcing functions used in these calculations were obtained from the expressions for an infinitely long constant phase velocity accelerator previously developed[2,6,8,13] and programed, recomputing them using the appropriate phase velocity and excitation at each axial station in the integration.

This procedure was used since application of the analysis in the appendix[14] to the present geometry and frequency indicated an error of only a few percent in so doing. The approximate equations thus obtained made calculation more simple. Thus the model having $\mu = \infty$ outside the coil was used to compare the approximate and exact calculation techniques, but $\mu = \mu_0$ was used in the calculations corresponding to experiment.

Assuming 1100 BTU/lb as a value for the enthalpy leaving the plasma source (representative of the accelerator off condition), a temperature of 5000°K can be found from the Mollier chart for argon.[16] Velocities were chosen by bracketing the value obtained using the measured mass flow and continuity. An inlet pressure of 1.6 Torr, inlet velocities of 2000–1550 m per sec, and inlet temperatures from 5000 to 7500°K were used as initial conditions for the computer program. Because of the uncertainty in flow properties and the differences between the equilibrium model and the actual nonequilibrium situation, a wide range of values was tried. The computed results which most closely approximated the observed values are shown in Figs. 8–10. The measured pressures and Mach numbers are also shown. The phase velocity curve in Fig. 8 was used in all computer runs and is a

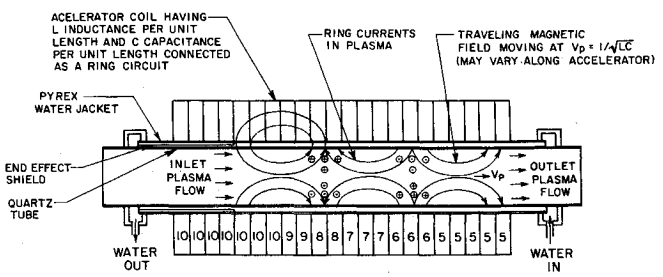


**Fig. 5 Final design of variable phase velocity traveling wave pump.**

†† The constant diameter channel was not chosen arbitrarily, but as an engineering compromise at the optimum configuration. Because the radial distribution of the volume force is nonuniform, $F_z \propto I_1^2(kr)$ as well as periodic[1] the boundary-layer problem is difficult; however, at the large Hartmann numbers and moderately small magnetic Reynolds numbers encountered in realistic accelerators, the boundary layers should be thin and slowly changing in the accelerator region. Also, numerical calculations using the one dimensional model[6,13,14] including viscosity indicate that the control of the thermodynamic process is more effective with variable phase velocity than with variable area.

**Table 1 Preliminary accelerator operating data**

| Run numbers | H68 | H69 | H70 | H71 | [a]H72 | [a]H74 | [a]H75 | [a]H76 | [a]H77 | [a]H78 |
|---|---|---|---|---|---|---|---|---|---|---|
| ($10^{-3}$ lb/sec) Mass flow (argon) | 3.4 | 3.4 | 3.4 | 3.4 | 3.4 | 3.6 | 3.6 | 3.4 | 3.4 | 3.4 |
| Plate voltage[b] | 7900 | 7950 | 7930 | 7950 | 7950 | 7850 | 7850 | 7850 | 7850 | 7830 |
| Plant current[b] | 1.3 | 1.5 | 1.5 | 1.5 | 1.5 | 1.8 | 1.8 | 1.8 | 1.8 | 1.8 |
| Helix and nozzle loss BTU/sec[b] | 2.23 | 4.46 | 5.95 | 5.15 | 5.59 | 1.98 | 5.64 | 2.60 | 4.0 | 6.3 |
| Estimated plate dissipation kw[b] | 5.9 | 6.4 | 6.4 | 6.4 | 6.4 | 7.3 | 7.3 | 7.8 | 7.8 | 7.8 |
| Estimated $h_0$ BTU/lb[c] | 690 | 397 | −48 | 196 | 67 | 1450 | 426 | 1180 | 732 | 78 |
| $P_5$ Torr | 10.5 | 13.5 | ... | ... | 13.5 | 12.5 | ... | 11.0 | 13.0 | 15.5 |
| $P_1$ Torr | 3.0 | 3.3 | 3.7 | 5.0 | 3.4 | 3.5 | 5.7 | 3.3 | 5.3 | 3.7 |
| $P_2$ Torr | 1.6 | 1.6 | 1.6 | 3.8 | 1.6 | 1.0 | 2.7 | 1.1 | 2.7 | 1.4 |
| $M_i$ ($\gamma$ = 1.67) | 0.97 | 1.0 | 1.10 | 0.58 | 1.05 | 1.44 | 1.04 | 1.30 | 0.96 | 1.2 |
| $M_i$ ($\gamma$ = 1.2) | 1.05 | 1.14 | 1.24 | 0.67 | 1.17 | 1.60 | 1.15 | 1.47 | 1.10 | 1.35 |
| $P_3$ Torr | 2.8 | 2.8 | 3.3 | 4.8 | 2.9 | 2.8 | 4.5 | 2.8 | 3.9 | 2.8 |
| $P_4$ Torr | 1.9 | 2.0 | 1.8 | 1.6 | 1.6 | 1.4 | 1.4 | 1.6 | 1.6 | 1.6 |
| $M_0$ ($\gamma$ = 1.67) | 0.70 | 0.65 | 0.91 | 1.30 | 0.89 | 0.97 | 1.35 | 0.83 | 1.13 | 0.83 |
| $M_0$ ($\gamma$ = 1.2) | 0.79 | 0.76 | 1.03 | 1.47 | 1.02 | 1.14 | 1.54 | 0.99 | 1.29 | 0.99 |
| Acceleration coil ring current amps rms | 0 | 0 | 132 | 213 | 0 | 0 | 220 | 0 | 211 | 0 |
| Coupling current amp rms | ... | ... | 25.0 | 42.0 | ... | ... | 46.0 | ... | 43.0 | ... |
| Plate voltage[d] | ... | ... | 12kv | 11kv | ... | ... | 11.0 | ... | 10.1 | ... |
| Plate current[d] | ... | ... | ... | 4.6 | ... | ... | 4.8 | ... | 4.4 | ... |
| Ampere turns/meter at accelerator inlet | ... | ... | 79,000 | 128,000 | ... | ... | 132,000 | ... | 126,000 | ... |
| Downstream water jacket heat transfer BTU/sec | 0.46 | 0.82 | 1.87 | 12.0 | ... | 0.48 | 13.0 | 0.57 | 11.0 | 1.8 |

[a] Small water leak at downstream end of accelerator channel.
[b] Plasma source section.
[c] At plasma source exit.
[d] Accelerator power supply.

best fit to the phase velocity measured on the accelerator with the high power amplifier at 50 amp rms.

The magnetic fields actually present in the accelerator can be calculated from the exciting current and the equations developed for the fields in the accelerator (Ref. 12, p. 37).

For Run 71, the approximate field amplitudes in Gauss are given below in Table 2.

It is interesting to note that from the impact pressure data, the accelerator outlet Mach number increased with accelerator power while the inlet Mach number decreased. The increase in downstream Mach number is in the expected direction. Apparently the fringing currents upstream of the inlet heat the flow and lower the inlet Mach number.

Because the limited instrumentation available did not permit measurement of all the properties of the plasma, a direct comparison with the predictions of the one-dimensional model cannot be made, however, the results show conclusively that large energy addition to a supersonic flow is possible while increasing Mach number and total pressure. There appears to be no effect which can account for the large observed increases in impact pressure $P_3$ and impact to static pressure ratio, $P_3/P_4$ in Runs H70, 71, 75, and 77 of Table 1, other than the operation of the accelerator in the anticipated mode of supersonic acceleration.

Considering the many simplifications of the theory and the scarcity of available data points, the agreement is considered reasonable. Clearly more data for a wider range of operating parameters is required for complete verification of the one-dimensional theory.

## Conclusions

Limitations of the available power supply for the accelerator limited a magnetic excitation to 130,000 amp turns per meter. However, at this level the Mach number at the accelerator outlet was increased from 0.75 without accelerator power to 1.5 with accelerator power. These results demonstrate the feasibility of coupling strongly to a gaseous plasma with a traveling magnetic field to increase both Mach Number and total pressure at supersonic velocities.

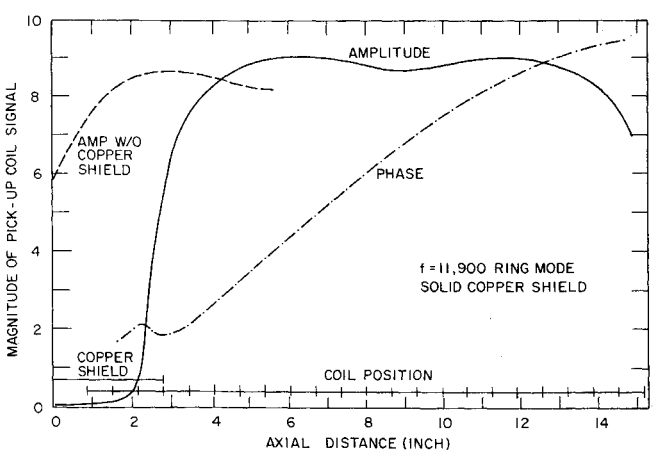


**Fig. 6 Amplitude vs distance with copper shield.**

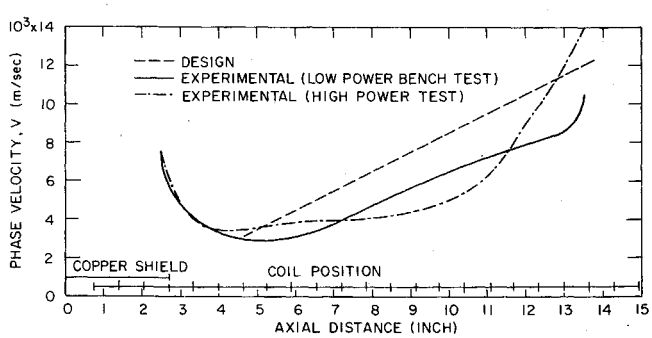


**Fig. 7 Phase velocity vs axial position for first order mode from bench test.**

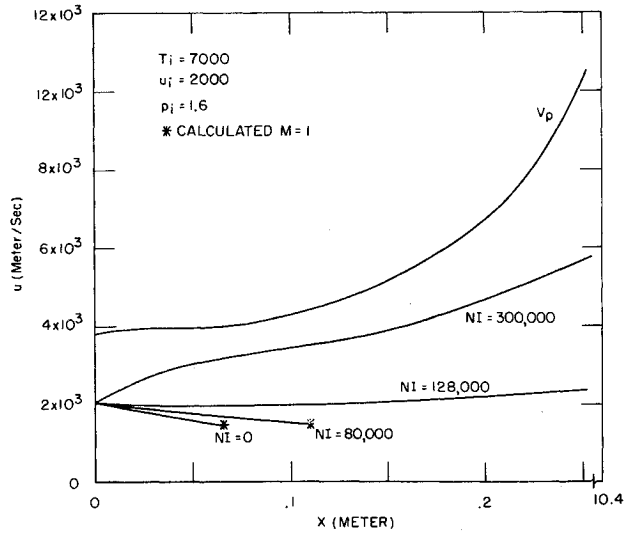


**Fig. 8 Velocity vs axial position.**

These results also indicate that the performance predicted in the earlier calculations is realistic or conservative, rather than over-optimistic with respect to over-all interaction.

The measured interaction is of the size and direction predicted by the one-dimensional variable phase velocity model developed for the fluid mechanic processes, giving credence to the calculations of performance using the model at the higher magnetic excitations required for high Mach number flight simulation.

## Appendix A: Calculation of the Vector Potential for a Finite Length Accelerator with Variable Phase Velocity

A cross section of the simplified model of the accelerator is shown in Fig. 11. (This is the same model used by Jester and Fanucci for constant phase velocity.[15])

Region 2, extending from $0 \leq z \leq L$ is the region of the applied current sheet and Regions 1 and 3 are the inlet and outlet regions. In order to simplify the algebra, the accelerator is assumed to be surrounded by a material of infinite permeability ($\mu = \infty$). The assumption implies that the strength of the field will be overestimated; however, the form of the fields will be the same. Thus the importance of the velocity gradient and end effect can be estimated from this model.

The effect of the exciting winding which is co-axial with the tube, for $0 \leq z \leq L$ (Region 2) and produces the traveling magnetic field is approximated by a purely aximuthal current sheet of radius $R$ and intensity $N(z)I$ surrounding the tube. The current sheet which is traveling in the $+z$ direction, has

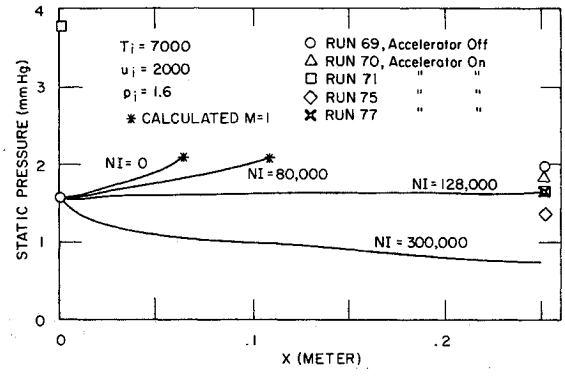


**Fig. 9 Static pressure vs axial position.**

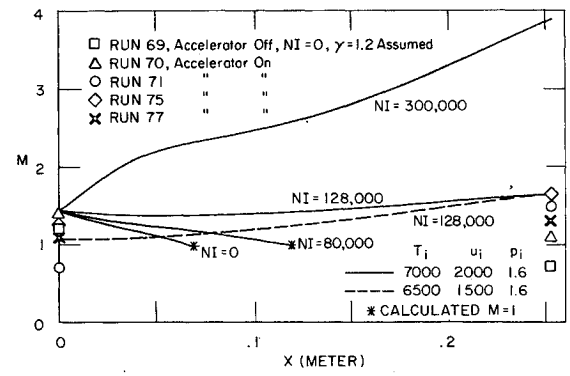


**Fig. 10 Mach number vs axial position.**

the form

$$\mathbf{K} = \hat{a}_\theta N(z) I Re\left[e^{i\left[\int_0^z k(\xi)d\xi - \omega t\right]}\right] \tag{A1}$$

The local phase velocity is then $V_p = \omega/k(z)$.

Under the assumption that the plasma does not affect the applied field, (small magnetic Reynolds number) the vector potential will have only an $\hat{a}_\theta$ component $A_\theta$ that must satisfy (also assuming a harmonic time dependence)

$$\nabla^2 A_\theta(r,z) - (1/r^2)A_\theta(r,z) = 0 \tag{A2}$$

with boundary conditions

$$\frac{1}{r}\frac{d}{dr}(rA_\theta)\bigg|_{r=R} = \begin{cases} \mu N(z) I \exp^{i\int_0^z k(\xi)d\xi} & 0 \leq z \leq L \\ 0 & z < 0,\ z > L \end{cases} \tag{A3}$$

As $z \to \pm\infty$ $A_\theta(r,z) \to 0$; and $A_\theta$ must be bounded at $r = 0$.

The aforementioned differential equation and boundary conditions can be solved by use of a Green's function.[17] The Green's function is found to be

$$G(r,z;r_0,z_0) = \begin{cases} \sum_{n=1}^{\infty} \dfrac{J_1(\lambda_n r_0/R)J_1(\lambda_n r/R)}{R^2[J_1(\lambda_n)]^2 k_n} e^{k_n(z-z_0)} & z < z_0 \\ \sum_{n=1}^{\infty} \dfrac{J_1(\lambda_n r_0/R)J_1(\lambda_n r/R)}{R^2[J_1(\lambda_n)]^2 k_n} e^{-k_n(z-z_0)} & z > z_0 \end{cases} \tag{A4}$$

where $r_0, z_0$ is the source point.

$A_\theta(r,z,t)$ is found by integrating $G(r,z;r_0,z_0)$ over the boundary. With the current sheet of Eq. (A1), the computation will involve integrals of the form

$$\text{integral} = \int N(z_0) \exp^{-k_n z_0 + i\int_0^{z_0} k(\xi)d\xi} dz_0 \tag{A5}$$

Successive integration by parts gives

$$\text{integral} = \frac{N(z_0) \exp^{-k_n z_0 + i\int_0^z k(\xi)d\xi}}{-k_n + ik(z_0)} \times \left(1 - \frac{[-k_n + ik(z)]1/N(z_0)\ dN/dz_0 - i\ dk/dz_0}{(-k_n + ik(z_0))^2} + \cdots\right) \tag{A6}$$

**Table 2 Approximate magnetic field amplitudes in Gauss for RUN H-71 (128000 at/m)**

| | Inlet | Exit |
|---|---|---|
| $B_{z(\text{wall})}$ | 390 | 260 |
| $B_z(r=0)$ | 120 | 220 |
| $B_{r(\text{wall})}$[a] | 300 | 100 |

[a] $B_{r(r=0)} = 0$.

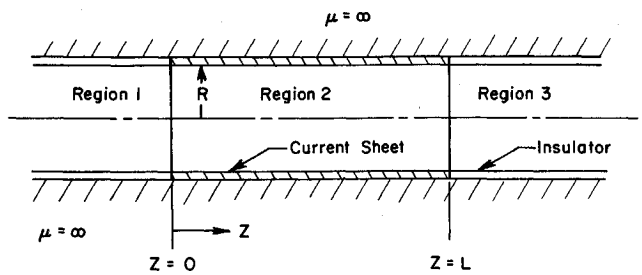


**Fig. 11 Simplified accelerator cross section.**

Only the first term of this series will be retained, since $N(z)$ and $k(z)$ are slowly varying functions of $z$. For a typical case

$$kR = 2 \quad L/R = 10 \quad d(kR)/d(z/L) = -\tfrac{2}{3}$$
$$d(N/N_0)/d(z/L) = -\tfrac{1}{2} \quad N/N_0 = \tfrac{1}{2}$$
$$\frac{[1/N(z_0)]dN(z_0)/dz_0}{[-k_n + ik(z_0)]} \sim \frac{1}{kR}\,\frac{1}{L/R}\,\frac{1}{N/N_0}\,\frac{d(N/N_0)}{d(z/L)} = 0.025 \tag{A7}$$

$$\frac{dk/dz_0}{[-k_n + ik(z_0)]^2} \sim \frac{1}{(kR)^2}\,\frac{1}{L/R}\,\frac{d(kR)}{d(z/L)} = 0.016$$

With these approximations, the vector potential $A_\theta(r,z)$ becomes

*Region 1*

$$A_\theta(r,z) = \sum_{n=1}^{\infty} \frac{(\mu I)J_1(\lambda_n r/R)}{R[J_1(\lambda_n)]k_n} \left\{ \frac{[k_n - ik(0)]N(0)}{k_n^2 + k^2(0)} \exp^{-k_n z} - \frac{[k_n + ik(L)]N(L)}{k_n^2 + k^2(L)} \exp^{-k_n(L-z)} \exp^{i\int_0^L k(\xi)d\xi} \right\} \tag{A8}$$

*Region 2*

$$A_\theta(r,z) = \frac{[\mu N(z) I]I_1[k(z)r]}{k(z)I_0[k(z)R]} \exp^{i\int_0^z k(\xi)d\xi} - \sum_{n=1}^{\infty} \frac{(\mu I)J_1(\lambda_n r/R)}{R[J_1(\lambda_n)]k_n} \left\{ \frac{[k_n - ik(0)]N(0)}{k_n^2 + k^2(0)} \exp^{-k_n z} - \frac{[k_n + ik(L)]}{k_n^2 + k^2(L)} N(L) \exp^{k_n(z-L)} \exp^{i\int_0^L k(\xi)d\xi} \right\} \tag{A9}$$

*Region 3*

$$A_\theta(r,z) = \sum_{n=1}^{\infty} \frac{(\mu I)J_1(\lambda_n r/R)}{R[J_1(\lambda_n)]k_n} \left\{ - \frac{[k_n - ik(0)]N(0)}{k_n^2 + k^2(0)} \times \exp^{-k_n z} - \frac{[k_n + ik(L)]}{k_n^2 + k^2(L)} \exp^{-k_n(z-L)} \exp^{i\int_0^L k(\xi)d\xi} \right\} \tag{A10}$$

In evaluating $A_\theta(r,x)$ in Region 2, the fact that

$$\frac{I_1[k(z)r]}{k(z)I_0[k(z)R]} = \sum_{n=1}^{\infty} \frac{2J_1(\lambda_n r/R)}{R[J_1(\lambda_n)][k_n^2 + k^2(z)]} \tag{A11}$$

was used to compute the first term. The fringing terms are eliminated by shielding as just explained. So, $A_\theta(r,z,t)$ in Region 2 is

$$A(r,z) = \frac{[\mu N(z) I]I_1[k(z)r]}{k(z)I_0[k(z)R]} \exp^{i\int_0^z k(\xi)d\xi} \tag{A12}$$

and the magnetic and electric fields are zero in Regions 1 and 3. With $k(\xi) = \text{const}$, this reduces to previous results.[1,2,10] The magnetic forcing terms $\mathbf{J} \times \mathbf{B}$ and $\mathbf{E} \cdot \mathbf{J}$ are easily calculated from the real part of the vector potential $A_\theta(r,z)$. For models with $L/R \geq 10$, $n_0/n_r \geq \frac{1}{2}$, and inlet shielding $k$ can be replaced by $k(z)$ and $n$ by $N(z)$, in the earlier results with an error of only a few percent.

## References


[1] Covert, E. E. and Haldeman, C. W., "The Traveling Wave Pump," *American Rocket Society Journal*, Vol. 31, No. 9, Sept. 1961, pp. 1252–1260.

[2] Covert, E. E., Boedeker, L. R., and Haldeman, C. W., "Recent Results of Studies of the Traveling Wave Pump," *AIAA Journal*, Vol. 2, No. 6, June 1964, pp. 1040–1046.

[3] Resler, E. L., Jr. and Sears, W. R., "The Prospects for Magneto-Aerodynamics," *Journal of the Aeronautical Sciences*, Vol. 25, No. 4, April 1958, pp. 235–245.

[4] Dahlberg, E., "On the One-Dimensional Flow of a Conducting Gas in Crossed Fields," *Quarterly of Applied Mathematics*, Vol. 19, No. 3, Oct. 1961, pp. 177–193.

[5] Boedeker, L. R., Coffin, J. R., Covert, E. E., and Haldeman, C. W., "Design and Evaluation of Radio Frequency Plasma Source, Part I: Self-Excited Oscillator," ARL Technical Rept. 67-0281, Dec. 1967, Aerospace Research Lab., USAF, Wright-Patterson AFB, Ohio.

[6] Haldeman, C. W., Sullivan, J. P., and Takahashi, H., "Initial Experiments with Electromagnetic Energy Addition to a Gas by a Traveling Magnetic Field," ARL Technical Rept. 70-0158, Sept. 1970, Aerospace Research Labs., USAF, Wright-Patterson AFB, Ohio.

[7] Seemann, G. R., Thornton, J. A., and Penfold, A. S., "An Experimental Investigation of the Electrodeless Traveling Wave Accelerator for Wind Tunnel Application," *AIAA Journal*, Vol. 8, No. 6, June 1970, pp. 1104–1111.

[8] Sullivan, J. P., "Design of a Variable Phase Velocity Traveling Wave Pump," MS thesis, May 1969, Dept. of Aeronautics and Astronautics, MIT.

[9] Messerle, H. K., "The Traveling-Wave Plasma Converter," *Journal of Fluid Mechanics*, Vol. 19, Part 4, Aug. 1964, pp. 577–590.

[10] Haldeman, C. W., "Unsteady Velocity Profiles in the Traveling Wave Pump," Sc.D. thesis Aug. 1964, Dept. of Aeronautics and Astronautics, MIT.

[11] Haldeman, C. W., "Harmonic Response Due to Compressibility in Traveling Wave Plasma Devices Possessing Cylindrical Symmetry," *The Physics of Fluids*, Vol. 9, No. 10, Oct. 1966, pp. 2074–2075.

[12] Boedeker, L. R., Coffin, J. B., Covert, E. E., and Haldeman, C. W., "Studies on Electromagnetic Means of Adding Heat and Kinetic Energy to a Gas," ARL Technical Rept. 65-121, June 1965, Aerospace Research Labs., USAF, Wright-Patterson AFB, Ohio.

[13] Haldeman, C. W. and Takahashi, H., "Further Studies on Electromagnetic Means of Adding Heat and Kinetic Energy to a Gas," ARL Technical Rept. 68-0115, July 1968, Aerospace Research Labs., USAF, Wright-Patterson AFB, Ohio.

[14] Haldeman, C. W. and Sullivan, J., "Engineering Aspects of Electromagnetic Energy Addition to a Gas by a Traveling Magnetic Field," ARL Technical Rept. 69-0148, Sept. 1969, Aerospace Research Labs., USAF, Wright-Patterson AFB, Ohio.

[15] Jester, J. L. and Fanucci, J. B., "Characteristics of a Finite Length MHD Traveling-Wave Cylindrical Accelerator or Generator," *AIAA Journal*, Vol. 7, No. 5, May 1969, pp. 864–870.

[16] LTV Research Group, "The Thermodynamic Properties of High Temperature Argon," Rept. RE-IR-26, Oct. 1961, LTV Aerospace Corp., Dallas, Texas.

[17] Morse, P. M. and Feshback, H., *Methods of Theoretical Physics*, McGraw-Hill, New York, 1953.